Sequential Exposure to IL21 and IL15 During Human Natural Killer Cell Expansion Optimizes Yield and Function

Caimei Zhang[1], Siddhant Kadu[1], Yansen Xiao[1], Omar Johnson[1], Andre Kelly[1,2], Roddy S. O'Connor[1,2], Meizan Lai[1], Hong Kong[1], Sriram Srivatsa[1], Victoria Tai[1], Eli Greenblatt[3], Matthew Holmes[3], James L. Riley[1,4], Carl H. June[1,2], and Neil C. Sheppard[1,2]

ABSTRACT

Natural killer (NK) cells are frequently expanded for the clinic using irradiated, engineered K562 feeder cells expressing a core transgene set of membrane-bound (mb) IL15 and/or mbIL21 together with 41BBL. Prior comparisons of mbIL15 to mbIL21 for NK expansion lack comparisons of key attributes of the resulting NK cells, including their high-dimensional phenotype, polyfunctionality, the breadth and potency of cytotoxicity, cellular metabolism, and activity in xenograft tumor models. Moreover, despite multiple rounds of K562 stimulation, studies of sequential use of mbIL15- and mbIL21-based feeder cells are absent. We addressed these gaps and found that using mbIL15- versus mbIL21-based feeder cells drove distinct phenotypic and functional profiles. Feeder cells expressing mbIL15 alone drove superior functionality by nearly all measures, whereas those expressing mbIL21 alone drove superior yield. In combination, most attributes resembled those imparted by mbIL21, whereas in sequence, NK yield approximated that imparted by the first cytokine, and the phenotype, transcriptome, and function resembled that driven by the second cytokine, highlighting the plasticity of NK cell differentiation. The sequence mbIL21 followed by mbIL15 was advantageous in achieving significant yields of highly functional NK cells that demonstrated equivalent *in vivo* activity to those expanded by mbIL15 alone in two of three xenograft models. Our findings define the impact of mbIL15 versus mbIL21 during NK expansion and reveal a previously underappreciated tradeoff between NK yield and function for which sequential use of mbIL21-based followed by mbIL15-based feeder cells may be the optimal approach in many settings.

Introduction

Natural killer (NK) cells are emerging as a promising adoptive cellular therapy platform for cancer (1). NK cells kill tumor cells in an antigen-independent manner following recognition of induced/stressed or missing self-antigens, which are common hallmarks of cancer stemming from metabolic stress and immune evasion (2). The cytotoxic potential of NK cells can also be enhanced and harnessed in an antigen-specific manner via antibody-dependent cellular cytotoxicity (ADCC) or engineering with chimeric antigen receptors (CAR; refs. 1, 2). Furthermore, NK cells play a key role in inducing antitumoral adaptive immunity via the secretion of chemokines that attract conventional type 1 dendritic cells (cDC1), the professional antigen-presenting cells most effective at cross-priming $CD8^+$ T-cell responses to tumors (3, 4). NK cells are especially suited for allogeneic use because donor-recipient mismatch in the killer Ig-like receptor (KIR) locus removes an inhibitory signal, and unlike T cells, NK cells lack the propensity to mediate GVHD (2). These facets of NK cell biology together with promising early safety and efficacy data in hematologic cancers underscore the promise of NK cell therapies (1).

Because NK cells are a minor population of circulating lymphocytes (5) and are typically used in the allogeneic setting at doses in the 10^9 range per infusion with several infusions in each patient (1), extensive *ex vivo* expansion is required (6–9). Multiple strategies have been applied for NK expansion, of which K562 cell-based feeder systems engineered to express a core transgene set of 41BBL together with membrane-bound (mb)IL15 and/or mbIL21 are the most common and achieve the greatest yields (6–12). Despite the widespread use of such K562 feeder cell lines, there have been only two head-to-head comparisons of K562 feeder cells expressing mbIL15 versus mbIL21 (7, 11) and no studies of sequential stimulation with these cytokines. Such comparisons are important as the IL15 and IL21 receptors signal predominantly via STAT5 and STAT3, respectively, resulting in differential outcomes (13). Available data show that 41BBL together with mbIL21 drives up to 60-fold greater NK yield than 41BBL with mbIL15, and that mbIL21 drives a less exhausted transcriptomic profile and longer telomeres (7, 11). Analyses of the direct functional activities of the resulting NK cells in these studies were limited to assays with a single HLA-negative cell line, which are typically highly sensitive to NK-mediated lysis, and no differences in cytotoxicity were observed (7, 11). Thus, important gaps remain in our understanding of the relative merits of mbIL15 versus, or in addition to, mbIL21, and nothing is known about the effects of their sequential use. We set out to address these gaps using methods not previously applied, including deep phenotyping by 28-color flow cytometry, to identify the resulting NK subpopulations, as well as broad functional assessments, including cytotoxicity, against a panel of tumor cell lines, 32-plex single-cell secretome analysis to assess polyfunctionality, metabolomic studies by Seahorse XF and related assays, and testing

[1]Center for Cellular Immunotherapies, University of Pennsylvania, Philadelphia, Pennsylvania. [2]Department of Pathology and Laboratory Medicine, Perelman School of Medicine, University of Pennsylvania, Philadelphia. [3]IsoPlexis, Branford, Connecticut. [4]Department of Microbiology, Perelman School of Medicine, University of Pennsylvania, Philadelphia, Pennsylvania.

Corresponding Author: Neil C. Sheppard, University of Pennsylvania, 3400 Civic Center Blvd, Philadelphia, PA 19104. E-mail: neil.sheppard@pennmedicine.upenn.edu

Cancer Immunol Res 2023;11:1524–37

doi: 10.1158/2326-6066.CIR-23-0151

in vivo in xenograft tumor models. Our K562 feeder cell lines expressed a core transgene set of CD64, 41BBL, and CD40 and varied in the expression of mbIL15 and/or mbIL21. We refer to these cells as K-IL15, K-IL21, and K-IL15-IL21. We reproduced prior data that mbIL21 drives superior NK cell yield, but we found this comes at a price of inferior antitumoral activity by every measure except ADCC, which was equal across all feeder cell conditions. The combination of mbIL15 and mbIL21 provided NK cell yields similar to mbIL21 and *in vitro* cytotoxicity similar to mbIL15, but reduced polyfunctional cytokine production eliminated the metabolic benefit conferred by mbIL15, and like NK cells expanded with mbIL21 alone, the resulting NK cells did not control tumors significantly in xenograft models. Sequential mbIL21 followed by mbIL15 imparted the respective benefits of both cytokines, with the resulting NK cells being equally effective as those expanded with mbIL15 alone in two of three xenograft models. These findings may have broad implications for optimizing the clinical translation of NK cell therapies.

Materials and Methods

Cell lines and cell culture conditions

Cell lines were purchased from the ATCC unless otherwise stated, authenticated by short tandem repeat profiling (ATCC), confirmed negative for *Mycoplasma* (Cambrex MycoAlert), and cultured in R10 medium [RPMI1640 (Gibco, 11875-085) supplemented with 10% heat-inactivated FCS (Avantor, catalog no. 97068-085), 1% Pen/Strep (Gibco, catalog no. 15140122), 1% Glutamax (Gibco, catalog no. 35050061; 2 mmol/L L-glutamine], 1% NEAA (Gibco, catalog no. 11140050), 1 mmol/L sodium pyruvate (Gibco, catalog no. 11360070), and 10 mmol/L HEPES (Gibco, catalog no. 15630130), except the engineered K562 feeder cell lines, which were cultured in R10 with 10% heat-inactivated human AB serum (Valley Biomedical, catalog no. HS1017HI). The passage numbers of cell lines used in this study are between 20 and 30. K562 is a chronic myelogenous leukemia cell line (CCL-243). U-251 MG is a primary glioblastoma tumor cell line (ECACC catalog no. 89081403). SKOV3 is an ovarian cancer cell line (HTB-77). RPMI 8226 is a multiple myeloma cell line (CCL-155). Raji is a B lymphoblast-like cell line (CCL-86). AsPC-1 is a pancreatic tumor cell line (CRL-1682). MM.1S is a B lymphoblast cell line (CRL-2974). For bioluminescence assays, Lentiviral vector pTRPE-encoding GFP-T2A-CBG was transduced to these cell lines for use in cytotoxicity assays or *in vivo* models as described previously (14). K562 feeder cell lines were produced by lentiviral transduction of the parental K562 cells with pTRPE-CD64, CD137 L (41BBL), CD40, and IL15/IL15Rα and/or mbIL21. GFP-positive tumor cell clones and the feeder cell clones were selected for high transgene expression following single-cell cloning via flow cytometry as discussed below.

NK cell purification and expansion

Peripheral blood mononuclear cells (PBMC) were obtained after written informed consent under University Institutional Review Board–approved protocols from healthy adult donors as described previously (15). NK cells were enriched from PBMCs via negative selection with Miltenyi Biotec's human NK Cell Isolation Kit (catalog no. 130-092-657) combined with LS column (Miltenyi Biotec, catalog no. 130-042-401) and MidiMACS Separator (catalog no. 130-042-302). NK cell isolation buffer was prepared by diluting MACS BSA Stock Solution (Miltenyi Biotec, catalog no. 130-091-376) 1:20 with autoMACS Rinsing Solution (Miltenyi Biotec, catalog no. 130-091-222). NK cell purities were achieved above 95% as assessed by flow cytometry as $CD3^{-}CD56^{+}$. K562 feed cells were irradiated with 100 Gy in an X-RAD 320ix cell irradiator (Precision x-ray). The purified NK cells were cocultured with irradiated K562 feeders at a 10:1 ratio of K562 feeders to NK cells in SCGM (CellGenix, catalog no. 20802-0500) supplemented with 10% heat-inactivated human AB serum, 2 mmol/L Glutamax, and 100 U/mL IL2 (Peprotech, #200-02) in G-Rex 6-well plate (Wilson Wolf, catalog no. 80240M). The cocultures were fed with 100 U/mL IL2 every 2 to 3 days, and the media were refreshed 75% on day 5 of each stimulation. On day 10 of the expansion, the expanded NK cells were stimulated a second time with irradiated feeders at the same feeders to NK cell ratio, and all *in vitro* assays and NK cell cryopreservation were performed on day 20 of the expansion. For NK cell cryopreservation, expanded NK cells were suspended in 100% CryoStor CS5 (STEMCELL, catalog no. 07933), frozen in an isopropanol-containing cryofreezing container at −80°C, and stored in a liquid nitrogen tank.

Cytotoxicity assay

NK cell cytotoxicity was determined by luciferase activity assessment as previously described with modification (16). K562-CBG, U251-MG-CBG, SKOV3-CBG, RPMI-8226-CBG, Raji-CBG, MM.1S-CBG, and AsPC-1-CBG were used as tumor target cells. Freshly isolated or expanded human NK cells were cocultured with tumor targets at ratios of 10:1, 3:1, 1:1, 1:3, and 1:10 of NK cells to tumor cells at 37°C overnight. The luciferase activity of tumor cells was assessed by reading luminescence with SpectraMax M3 Multi-Mode Microplate Reader (Molecular Devices) reader after adding substrate luciferin (Caliper Part no.: 122796). For the glycolysis dependence of NK cell cytotoxicity, NK cells were pretreated with/or without 20 mmol/L 2-deoxy-D-glucose (2-DG) at 37°C overnight, followed by washing with PBS to remove residual 2-DG before coculture with K562-CBG at a ratio of 1:1 overnight. NK cell ADCC was determined in the presence of the HER2 antibody trastuzumab (Roche, catalog no. HY-P990; 2 μg/mL) in cocultures with SKOV3-CBG cells (naturally express HER2 antigen) at an NK cell:tumor cell ratio of 3:1 in RPMI1640 with 4% low IgG serum (Gibco, A3381901) at 37°C overnight.

Isoplexis single-cell 32-plex secretome assay

Expanded NK cells were activated with the TLR7/8 agonist R848 (InvivoGen, catalog no. tlrl-r848; 1 μg/mL) overnight. Activated NK cells were then stained with CellTrace Violet dye (Isoplexis, catalog no. STAIN-1001-1) and 30,000 NK cells were loaded into an IsoCode chip (Isoplexis, catalog no. ISOCODE-3L03-4) for the single-cell secretome assay with Isoplexis-Isospark instrument. A total of 500–1,400 qualified single cells were analyzed, and cytokines secreted by ≥2% of the population were calculated for the polyfunctional strength index (PSI). PSI was defined as the percentage of polyfunctional cells (secreting two or more proteins) in a sample, multiplied by the average signal intensity of the secreted proteins from individual functional groups from each cell.

ELISAs

Expanded NK cells were cocultured with/or without tumor target K562 cells at effector-to-target (E:T) ratio 1:1 overnight. Centrifuged the plates 1,500 rpm at room temperature for 5 minutes, and the supernatants were transferred into a new plate and stored at −80°C until the time of assay. The secretion of INFγ, TNFα, and GMCSF by NK cells were measured by ELISA using BD OptEIA Human IFNγ ELISA Set (catalog no. 55142), BD OptEIA Human TNF ELISA Set (catalog no. 555212), and BD OptEIA Human GM-CSF ELISA Set (catalog no. 555126), respectively, following the manufacturer's

instruction. The absorbance was read at 450 nm with a Multi-Mode microplate reader (Agilent BioTek Synergy H1).

Seahorse metabolism assay

Mitochondrial stress tests were performed on expanded NK cells using Seahorse XFe24 Analyzer (Agilent Technologies) with Seahorse XF Cell Mito Stress Test Kit (Agilent Technologies, catalog no. 103015-100), according to the manufacturer's instructions. Briefly, NK cells were collected at the end of expansion and resuspended in Seahorse XF medium (Agilent Technologies, catalog no. 103576-100) after being washed once with Seahorses XF medium. A total of 125,000 NK cells/well were plated into PDL-coated XF 96-well microplates (Agilent Technologies, catalog no. 103730-100), and cells were incubated in CO_2-free conditions for 1 hour before loading into the instrument. Oxygen consumption rate (OCR) and extracellular acidification rate (ECAR) were measured under basal conditions, followed by the sequential injections of oligomycin (Oligo; 1 μmol/L), FCCP (1 μmol/L), and rotenone (Rot; 500 nmol/L) plus antimycin (Ant; 500 nmol/L). This procedure allows the accurate calculation of oxygen consumption from basal respiration, spare respiratory capacity (SRC), and ATP production, as well as an estimation of extracellular acidification from basal glycolysis, and glycolytic capacity of cells.

Bulk RNA sequencing

RNA was extracted from freshly isolated human NK cells and expanded NK cells using the QIAGEN RNeasy Mini Kit (QIANGEN, catalog no. 74106) following the manufacturer's instructions, and samples were processed by Novogene for sample quality, library preparation, sequencing, and data analysis. RNA purity was determined using a NanoDrop 2000/2000c: A260/280 = 1.8–2.2; A260/230 ≥ 1.8. RNA integrity was determined with an Agilent 2100 Bioanalyzer: RNA integrity number ≥ 5.8, with smooth base line. A nondirectional library was prepared using Illumina Stranded mRNA Prep (catalog no. 20040534) following the manufacturer's instruction. The library was checked with a Qubit Flex Fluorometer (Invitrogen), by real-time PCR for quantification, and a bioanalyzer was used for size distribution detection. Quantified libraries were pooled and sequenced on Illumina platform NovaSeq 6000 S4 flowcell, according to effective library concentration and data amount.

For data analysis, clean data were obtained by removing reads containing adapter, ploy-N, and low-quality reads from raw data. All the downstream analyses were based on clean data. Clean reads were aligned to the reference genome (hg38) using Hisat2 v2.0.5. Feature Counts v1.5.0-p3 was used to count the uniquely mapped gene, and the fragments per kilobase per million mapped reads of each gene was then calculated on the basis of the length of the gene and read counts mapped to the gene. Differential expression analysis was performed using the DESeq2R package (1.20.0). A corrected *P* value of 0.05 and an absolute fold change of 2 were set as the threshold for significant differential expression. Gene set enrichment analysis (GSEA) was performed using Software GSEA 4.3.2 with the gene sets from the MSigDB database-c2.cp.kegg.v2022.1.Hs.symbols.gmt. The FDR cutoff was set as 0.25.

Murine xenograft models

All animal studies were performed under an approved Institutional Animal Care and Use Committee protocol at the University of Pennsylvania (Philadelphia, PA). NOD/scid/IL2rγ−/− (NSG) mice originally obtained from The Jackson Laboratories were bred and maintained by the Stem Cell and Xenograft Core at the University of Pennsylvania in pathogen-free conditions. Eight to 10 weeks old male mice were used for the studies. We utilized a previously reported intravenous disseminated Raji cell Burkitt lymphoma model (17), an intraperitoneal carcinomatosis outgrowth model (18) modified to use U251 glioblastoma cells, and an in-house developed intraosseous RPMI-8226 multiple myeloma model. Briefly, for the Raji cell Burkitt lymphoma model, 40 NSG mice received intravenous injection of 1×10^5 Raji cells/mouse in 200 μL PBS. On day 2 after Raji cell injection, frozen expanded NK cells from different conditions (K-IL15, K-IL21, K-IL15-IL21, and K-IL21-K-IL15) were thawed, and 15×10^6 cells/mouse in 200 μL PBS were intravenously injected (8 mice/group). Control mice were injected with PBS. For the intraosseous RPMI-8226 multiple myeloma model, NSG mice were preconditioned with busulfan (30 mg/kg i.p. injection) before receiving an intraosseous injection of RPMI-8226-CBG cells (2×10^6 cells/mouse in 10 μL PBS). On day 4 of tumor engraftment, mice received intravenous injection with freshly expanded NK cells from different conditions (20×10^6 cells/mouse). Thereafter at weekly intervals on day 11 and day 18 following tumor injection, mice received a second and third dose of frozen expanded NK cells from two different donors (20×10^6 cells/mouse). Meanwhile, human recombinant (r)IL2 (12,500 IU/mouse) was intraperitoneally delivered to the mice twice per week, starting 1 day prior to NK cell injection. For the intraperitoneal carcinomatosis outgrowth model, 45 NSG mice received intraperitoneal injections of U251-CBG cells [1×10^6 cells/mouse in 100 μL X-Vivo-10 (Lonza, catalog no. BE04-380Q)], followed by intraperitoneal injection of NK cells from different conditions (3×10^6 cells/mouse in 100 μL X-Vivo-10) 5 hours later (10 mice per group, except for the K-IL15-IL21 group that had 5 mice due to low NK cell yield of that particular expansion). Tumor growth was monitored by bioluminescence imaging (BLI) twice a week. For tumor BLI, mice were anesthetized using PerkinElmer's XGI-8 Gas Anesthesia System and intraperitoneally injected with D-luciferin, Firefly, potassium salt (Caliper Part no.: 122796; 150 mg/kg) in PBS. Tumors were imaged with IVIS Lumina III In Vivo Imaging System 12 minutes after D-luciferin injection. Images were analyzed with the Living Image v4.7 software, and the total tumor flux was used to compare tumor growth.

Tissue dissociation

On day 4 after NK cell intravenous injection, human NK cells in mouse peripheral blood, bone marrow, spleen, and lung were detected with anti-hCD45-BV785 (BioLegend, catalog no. 304048) and counted using BD Trucount tubes (catalog no. 663028). For collecting blood, mice were fully anesthetized, and approximately 100 μL blood was collected by retro-orbital bleeding using a microhematocrit capillary tube (BD, catalog no. 420316) into BD Microtainer Blood Collection Tube containing K_2 EDTA Additive (BD, catalog no. 365974), and 50 μL was used for BD Trucount staining. Bone marrow immune cells were isolated from mouse femur bone marrow. Briefly, mice were euthanized with CO_2 and hind femurs were collected. Bone marrow was collected using centrifugation and resuspended in 0.5 mL RPML1640. Bone marrow cells were filtered through a 70-μm cell strainer and washed with 0.5 mL RPML1640 medium. Samples were centrifuged at 1,500 rpm at room temperature for 5 minutes. The pellets were resuspended in 0.5 mL 1x red blood cell (RBC) lysis buffer (BD Biosciences, catalog no. 349202) and incubated at room temperature for 15 minutes. After centrifugation, the pellets were resuspended with 100 μL FACS buffer (2% FBS in PBS) and prepared for Trucount staining as discussed. Mouse splenocytes were isolated by processing the spleen through a 70-μm cell strainer, followed by red cell lysis with BD FACS Lysing Solution. After centrifugation, the pellets were

resuspended with FACs buffer and prepared for Trucount staining. Lung tissues were digested with Miltenyi Biotec's Lung Dissociation Kit, mouse (catalog no. 130-095-927) using Miltenyi Biotec's gentleMACS Octo Dissociator with heaters. After digestion, the cell suspensions were filtered with 70-μm cell strainers, followed by RBC lysis. After centrifugation, the pellets were resuspended with FACs buffer and prepped Trucount staining.

Flow cytometry

Human freshly isolated and expanded NK cells or feeders were blocked with Human TruStain FcX (BioLegend, catalog no. 422302) for 10 minutes preceding the antibody staining. Anti-hIL15Ra-FITC (Thermo Fisher Scientific, catalog no. 11-7159-42), anti-CD40-PE (BD Biosciences, catalog no. 555589), anti-CD64-PE-Cy7 (BioLegend, catalog no. 305022), anti-hIL21-AF647 (BioLegend, catalog no. 513006), and anti-h41BBL-BV421 (BioLegend, catalog no. 309820) were used for assessing the transgene expression on K562 feeder cells. NK cell viability was assessed by AnnexinV-PE (BD Biosciences, catalog no. 556422) and 7-AAD (Thermo Fisher Scientific, catalog no. 00-6993-50) staining. The yields of NK cell expansion were determined by flow cytometry with CountBright Absolute Counting Beads (Life Technologies, catalog no. C36950) and 7-AAD, CD3, and CD56 staining. The following antibodies were used for NK cell phenotyping: anti-hCD3-PE-Cy5 (BioLegend, catalog no. 300310), anti-hCD56-PE (BioLegend, catalog no. 318306), anti-hCD16-APC (BioLegend, catalog no. 302012), anti-hNKp46-AF700 (catalog no. 331932), anti-hNKG2D-APC-Cy7 (BioLegend, catalog no. 320824), anti-hCD158b-FITC (BioLegend, catalog no. 312604), anti-hCD253-PE-Cy7 (BioLegend, catalog no. 308216), anti-CD96-PE-Cy7 (BioLegend, catalog no. 338416), anti-hSiglec-7-APC/Fire750 (BioLegend, catalog no. 339208), anti-hTIM3-BV711 (BioLegend, catalog no. 345024), anti-hCD220R-PE-Cy7 (BioLegend, catalog no. 329312), anti-hLAG3-BV650 (BioLegend, catalog no. 369316), ant-PD1-BV605 (BioLegend, catalog no. 329924), anti-TIGIT-APC-Cy7(BioLegend, catalog no. 372734), anti-hCD98-FITC (BioLegend, catalog no. 315603), anti-CD71-AF700 (BioLegend, catalog no. 334130), anti-hNKp30-BV711 (BD Biosciences, catalog no. 563383), anti-hNKp44-BV650 (BD Biosciences, catalog no. 744302), and anti-hCD178-BV605 (BD Biosciences, catalog no. 744099). Data were acquired on BD LSRFortessaTM Flow Cytometer (Becton Dickinson) and analyzed with Flowjo_v10.8.1 software.

The NK panel for the 28-color FACSymphony A5 flow cytometer (BD Biosciences) was developed as described previously (19). See Supplementary Table S1for antibodies used. Data were processed and analyzed with Flowjo_10.8.1 software, using PhenoGraph clustering coupled with Uniform Manifold Approximation and Projection (UMAP) visualization following cleaning with FlowAI. A total of 50,000 cells of clean data per sample were used for PhenoGraph clustering.

Statistical analysis

Data are presented as mean ± SEM. All statistical analyses were performed with GraphPad Prism software for Windows v9.0.1 (GraphPad). Statistically significant differences were tested by the specific tests indicated in the figure legends. A P value less than 0.05 was considered significant. Where used for statistical evaluations, figure legends clarify whether ANOVA was one-way or two-way, or fitting mixed model.

Data availability statement

To access original data, please contact the corresponding author. Bulk RNA sequencing (RNA-seq) data are available in Gene Expression Omnibus at GSE234384.

Results

Comparative NK yields using mbIL21 and/or mbIL15 alone or sequentially

K562 feeder cell lines were developed by lentiviral transduction of the K562 wild-type (WT) cells with CD64, 41BBL, CD40, IL15Rα/IL15 or/and mbIL21, with the latter construct as described previously (ref. 20; Supplementary Fig. S1A), followed by single-cell cloning and characterization (ref. 21; **Fig. 1A**). Of these transgenes, CD64, 41BBL, and the mb cytokines have been extensively used in K562 feeder cells for NK expansion as part of core transgene sets (6–9, 11, 12), but CD40 has not. The CD40-CD40 ligand (CD40L) pair is well characterized as signaling into the $CD40^+$ cell, for example in the licensing of dendritic cells by T cells, but CD40 L is capable of reverse signaling upon engagement of CD40, which in T cells enhances proliferation and maturation (22). Because CD40 L is also expressed in activated NK cells (23, 24), we investigated K562 cells expressing CD40, and found they enhanced the selective expansion of NK cells from PBMCs, as well as NK cell yield when starting with purified NK cells, with promising trends toward improved NK cytotoxicity (Supplementary Fig. S1B–S1I). We therefore included CD40 in our core transgene set. To identify optimal NK expansion conditions, we explored recursive stimulation with the K562 feeder cells (**Fig. 1B**). By monitoring the NK cell volume and population doubling after feeder cell stimulation, we selected day 10 as the timepoint for a second feeder cell stimulation (**Fig. 1C**). There were no significant differences in NK cell viability among the different expansion conditions. However, for some donors, exposure to K-WT or sequential K-IL15-K-IL21 resulted in elevated NK cell apoptosis at day 20 of the expansion (**Fig. 1D**; Supplementary Fig. S2A). Our expanded NK cells were highly pure at the end of the expansion with contaminating $CD3^+$ T cells accounting for < 0.02% of the product across all conditions (Supplementary Fig. S2B). Consistent with prior findings (7), expansions of NK cells with K-IL21 resulted in significantly higher yields [counted by excluding 7-AAD–positive cells (Supplementary Fig. S2C)] than stimulation with K-IL15 at both day 10 (∼600- to 1,200-fold vs. ∼100- to 600-fold) and day 20 (15,000- to 700,000-fold vs. ∼1,000- to 15,000-fold). Stimulation with K-IL15-IL21 resulted in similar NK expansion compared with stimulation with K-IL21 (**Fig. 1E**). In the first report to our knowledge of NK expansion with sequential feeder cell types, K-IL15-K-IL21 or K-IL21-K-IL15 achieved NK yields that fell between the K-IL15 condition and K-IL21 condition, and the K-IL21-K-IL15 condition resulted in significantly greater NK expansion compared with the opposite order (∼11,000- to 500,000-fold vs. ∼2,000- to 110,000-fold; **Fig. 1E**), with a trend toward higher viability (**Fig. 1D**).

The phenotypic profile of expanded NK cells is influenced by the type and sequence of mb-cytokine stimulation

The canonical subtypes of NK cells are defined by the expression of CD56 and CD16. The two dominant subtypes are $CD56^{bright}CD16^{dim/-}$, which produce more cytokines, and $CD56^{dim}CD16^+$ that are more cytotoxic (25). However, the pattern of these canonical markers and their relation to functional potency are uncoupled following expansion (26), with $CD56^{bright}CD16^+$ expanded NK cells having a superior antitumor function (27, 28). In line with prior reports (11, 26), we found CD56 was upregulated, whereas CD16 was downregulated in expanded NK cells from all conditions compared with freshly isolated NK cells (**Fig. 2A–C**). Expansion by any feeder cell, including K-WT, led to a dominant $CD56^{bright}CD16^+$ population, and only repeated use of the mbIL21-expressing feeders K-IL21 or K-IL15-IL21 resulted in diversity of CD56 expression, with approximately 30% $CD56^{dim}CD16^+$ NK cells for most

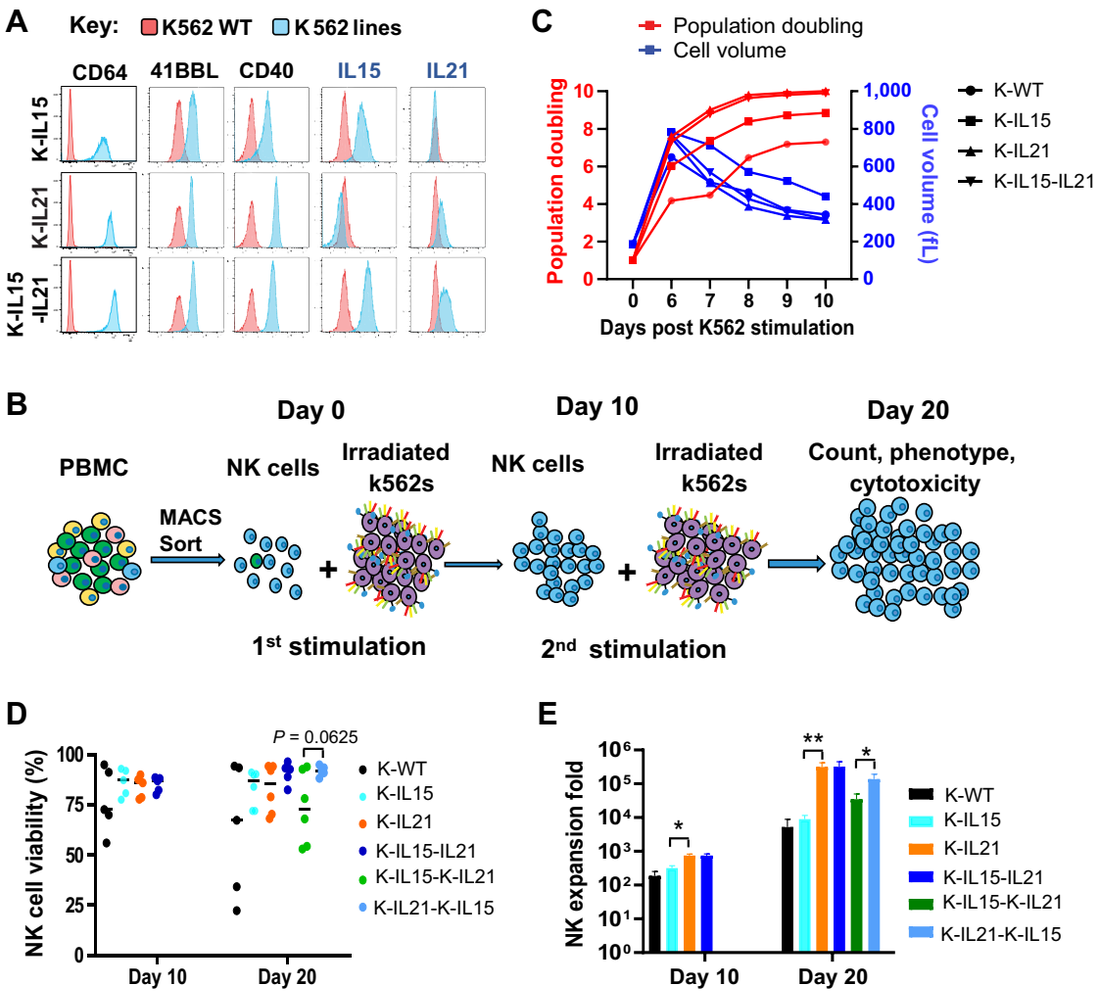

Figure 1.

Exposure to K562 expressing mbIL21 gives superior NK yield. **A,** Surface expression of CD64, 41BBL, CD40, IL15, and IL21 on the K562 feeders (K)-IL15, K-IL21, and K-IL15-IL21. **B,** Workflow of our NK cell expansion process. On day 10, NK cells were repeatedly stimulated with either the same type of feeders or switched from K-IL15 to K-IL21 and vice versa. **C,** Dynamic population doubling and cell volume of NK cells after K562 feeder exposure. **D,** Viability of NK cells on day 10 and day 20 of the expansion was determined by staining with Annexin V-PE and 7-AAD (5–6 donors). **E,** Expansion fold of NK cells on day 10 and day 20 from 11 donors, except for K-WT from 5 donors. The results are expressed as mean ± SE; *, $P < 0.05$ and **, $P < 0.01$ by fitting mixed model with multiple paired t test.

donors (**Fig. 2A** and **B**). The mean fluorescence intensity (MFI) for CD16 was reduced approximately 4- to 5-fold in all expansion conditions (**Fig. 2C**). Because CD16 shedding on activated NK cells results from the action of ADAM17 and/or MMP25 (29, 30), we examined transcript levels via bulk RNA-seq and found *CD16* and *ADAM17* mRNAs were unchanged, whereas *MMP25* mRNA was upregulated in expanded NK cells (Supplementary Fig. S3A).

Using 28-color flow cytometry analysis to gain deeper insight into the phenotypic diversity of the expanded NK cells, we observed 20 distinct subpopulation clusters, with the greatest distinction of the distribution of clusters between K-IL15 and K-IL21 conditions (**Fig. 2D**). NK cells expanded with K-IL15-IL21 and K-IL15-K-IL21 both showed similarity to the K-IL21 condition, whereas K-IL21-K-IL15 had a similar subpopulation distribution to K-IL15 (**Fig. 2D**). Expansion with K-IL15 or K-IL21-K-IL15 enhanced the abundance of clusters 3, 10, 11, and 12, which were characterized by high expression of CD56 and the cytotoxicity receptors NKG2D, NKp46, NKp30, and NKp44, as well as the suppressive receptor NKG2A. Expansion with K-IL21, K-IL15-IL21, and K-IL15-K-IL21 enhanced the abundance of clusters 1, 4, 5, and 7 that were characterized by generally lower expression of CD56, NKG2D, NKp30, NKp44, and NKp46, with cluster 7 having high expression of KIRs (CD158; **Fig. 2D–F**). These phenotypic findings suggest the K-IL15 and K-IL21-K-IL15 conditions endow expanded NK cells with greater sensitivity to tumor cells via enhanced expression of various cytotoxicity receptors than expansion with K-IL21, K-IL15-IL21, or K-IL15-K-IL21.

Using flow cytometry, we additionally observed significant upregulation of the activating receptors NKp44, NKp30, NKG2D, and the cell death ligands FasL and TRAIL in expanded NK cells, in terms of both the percentage and the MFI, except for NKG2D where only the percentage was significantly elevated compared with freshly isolated NK cells (**Fig. 2G**; Supplementary Fig. S3A and S3B). K-IL15 exposure led to significantly higher expression of NKp30 (percentage and MFI), NKp44, and TRAIL (percentage) compared with K-IL21 exposure

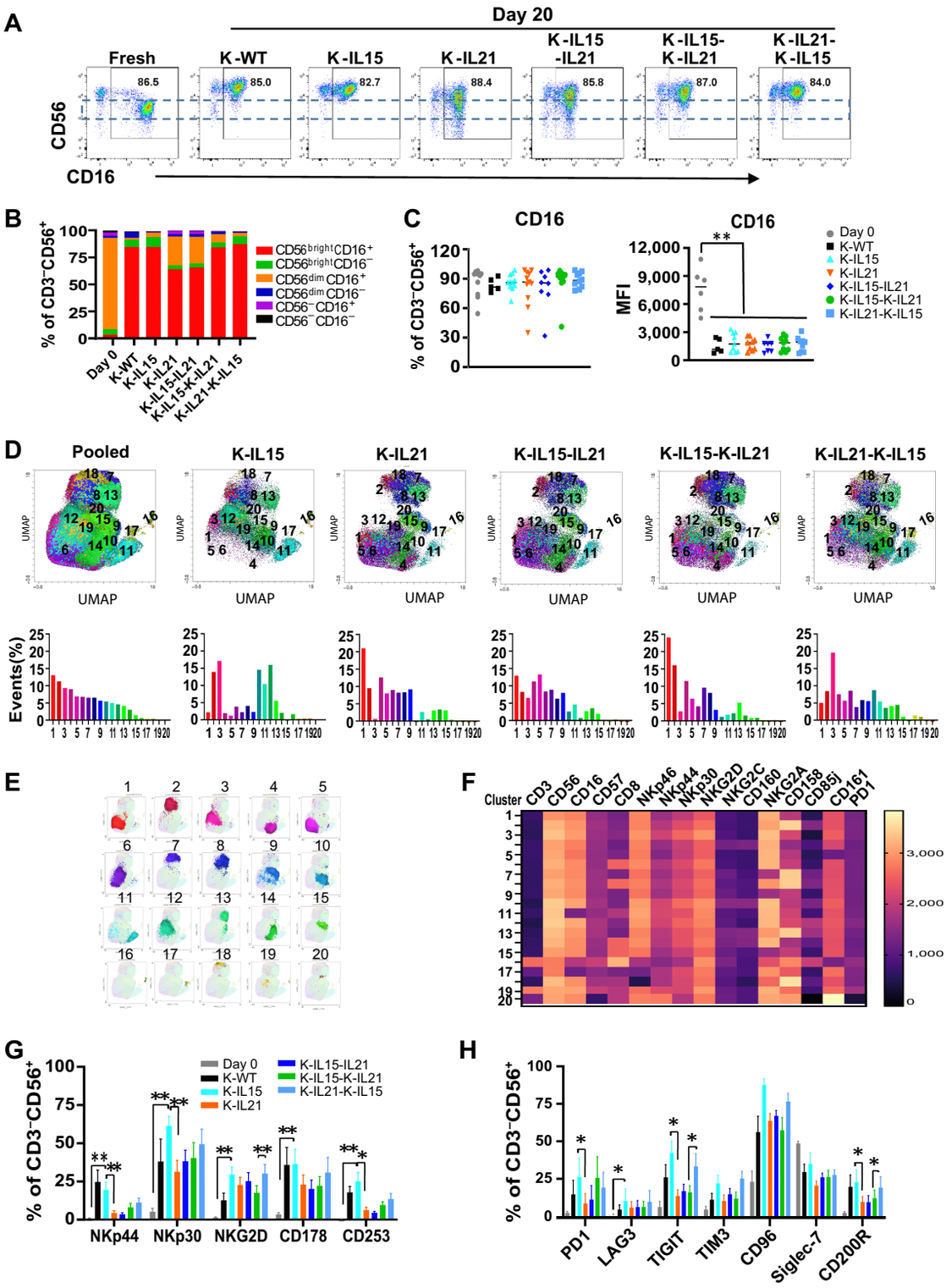

Figure 2.

The distinct phenotype of NK cells from different stimulation conditions. **A,** Representative flow plots of CD56 and CD16 expression on freshly isolated NK cells and expanded NK cells. **B,** The percentages of different NK cell subsets based on the expression of CD56 and CD16 in freshly isolated NK cells and expanded NK cells ($N = 4$ donors). **C,** The percentage and MFI of CD16 ($N = 6$–11 donors). **, $P < 0.01$ by one-way ANOVA with paired t tests. **D–F,** 28-color flow cytometry analysis (from 1 of 2 donors, the other donor showed similar results) showing the subpopulations of expanded NK cells. UMAP (top) and the quantification of clusters (bottom; **D**), individual clusters (**E**), and the heat map of protein surface expression in the individual cluster (**F**). Pooled: the combination of cells from five groups. The percentage of activating receptors (NKp44, NKp30, and NKG2D), cell death ligands (CD178 and CD253; **G**; $N = 10$ donors), and inhibitory receptors (PD1, LAG3, TIGIT, TIM3, CD96, Siglec-7, and CD200R; **H**; $N = 7$ donors) in freshly isolated NK cells and expanded NK cells. The results are expressed as mean ± SE; *, $P < 0.05$ and **, $P < 0.01$ by a two-way ANOVA with multiple paired t test.

(**Fig. 2G**; Supplementary Fig. S3B and S3C). NK cells expanded with sequential K-IL21-K-IL15 showed significantly greater percentage expression of NKG2D than those expanded with K-IL15-K-IL21 (**Fig. 2G**). The expression of the immune checkpoint markers increased upon NK expansion, except for SIGLEC-7. NK cells expanded with K-IL15 or K-IL21-K-IL-5 had significantly greater percentage expression of PD-1 (K-IL15 only), TIGIT, and CD200R than those expanded with K-IL21 or K-IL15-K-IL21, respectively (**Fig. 2H**; Supplementary Fig. S4). The observed profiles suggest that NK cells expanded with K-IL15 or K-IL21-K-IL15 are more activated and better able to sense stress ligands and kill tumor cells than those from other expansion conditions.

Expansion with K-IL15 or K-IL21-K-IL15 enhances the breadth and potency of NK cytotoxicity and polyfunctional cytokine production

To assess the cytotoxic potential of the expanded NK cells, we used WT K562 cells as targets (**Fig. 3A**) and extended our observations to a panel of six tumor cell lines derived from various solid and hematologic malignancies that showed variable sensitivity to freshly isolated NK cells (**Fig. 3B**). We defined target cells as sensitive to freshly isolated NK cells if they showed ≥ 50% killing over two or more E:T ratios, and partially or fully resistant if there was ≤ 50% or ≤ 10% killing, respectively, at an E:T ratio of 10:1. According to these criteria, RPMI-8226 multiple myeloma cells were sensitive, whereas U251 glioma cells were partially resistant, and Raji Burkitt lymphoma, MM.1S multiple myeloma, AsPC1 pancreatic cancer, and SKOV3 ovarian cancer cells were fully resistant to freshly isolated NK cells (**Fig. 3B**). Expanded NK cells exhibited greater cytotoxic activity against tumor targets that were sensitive or partially resistant to freshly isolated NK cells, but only those expanded by K-IL15 and K-IL21-K-IL15, and to a lesser extent K-IL15-IL21, showed activity against target cells fully resistant to fresh NK cells (**Fig. 3A** and **B**; Supplementary Fig. S5A). For most donors, switching from K-IL21 to K-IL15 increased cytotoxicity, whereas the inverse sequence decreased cytotoxicity (Supplementary Fig. S5B). NK cells expanded with sequential K-IL21-K-IL15 were profoundly more cytotoxic than those expanded with the inverse sequence of K-IL15-KIL21, which trended toward lower cytotoxicity than NK cells grown with K-IL21. CD107a expression supported the cytotoxicity findings (Supplementary Fig. S5C). To assess ADCC, we used the Her2 mAb trastuzumab and $Her2^+$ SKOV3 and $Her2^-$ U251 cells (**Fig. 3C**). The addition of trastuzumab to the U251 cells did not affect target cell killing, whereas the average cell lysis of SKOV3 was significantly elevated with all expanded NK cells, especially for those expanded with genetically engineered feeder cells (**Fig. 3C**), despite the uniform decrease in CD16 expression across all feeder cell conditions (**Fig. 2C**).

NK cells orchestrate antitumoral immune responses via the production of cytokines and chemokines (3, 4). We therefore measured the production of GMCSF, TNFα, and IFNγ in response to K562 target cells in the media by ELISA. There were no differences in IFNγ production, but we found statistically significant increases in the production of TNFα and GMCSF by K-IL15–expanded NK cells compared with K-IL21–expanded NK cells, with nonsignificant trends for K-IL21-K-IL15 compared with K-IL21 or K-IL15-K-IL21 (**Fig. 3D**). Because polyfunctional lymphocytes secreting ≥2 cytokines are more effective than monofunctional cells (31), we next explored the single-cell secretome of NK cells stimulated with the TLR7/8 agonist R848 (**Fig. 3E**; Supplementary Fig. S6A and S6B). The PSI, a potential correlate of *in vivo* activity (32), is defined as the percentage of polyfunctional cells in a sample, multiplied by the average signal of each factor. NK cells expanded with K-IL15 achieved the highest PSI, followed by NK cells expanded with sequential K-IL21-K-IL15 (**Fig. 3E**). NK cells expanded with K-WT showed the lowest PSI, indicating the importance of the various transgenes in the K562 feeders to impart polyfunctional activity on the expanded NK cells. Expansion with K-IL15-IL21 gave surprisingly poor polyfunctionality, with a lower PSI than achieved by expansion with K-IL15 or K-IL21 alone or in either sequence (**Fig. 3E**). Three-dimensional t-distributed stochastic neighborhood embedding analysis showed distinct clustering based on expansion conditions, with the K-IL15 and K-IL21 conditions being most distal to one another, K-IL15-IL21 in the middle, and K-IL21-K-IL15 most similar to K-IL15 (Supplementary Fig. S6A). Polyfunctional heat map analysis identified a total of 40 distinct polyfunctional subpopulations across all conditions, with NK cells expanded by K-WT having 12 polyfunctional populations and lacking a prominent RANTES-dominant subpopulation, whereas those expanded by engineered feeder cells had 17 to 22 polyfunctional subpopulations each (Supplementary Fig. S6B).

Feeder cell expansion conditions imprint distinct metabolic profiles on expanded NK cells

Cellular metabolism is tied to the differentiation and education of NK cells, as well as their fate in the tumor microenvironment (18, 33). To determine the metabolic profile of expanded NK cells, we performed a Seahorse assay to simultaneously measure OCR and ECAR as indices of mitochondrial function and glycolysis, respectively (34). Baseline OCR and ECAR trended toward an increase in NK cells expanded with K-IL15 alone relative to those in NK cells expanded with K-WT (**Fig. 4A** and **B**). The mitochondrial SRC was highest in K-WT (**Fig. 4A**). This phenotype was maintained by K-IL15 stimulation and significantly attenuated in all regimens containing mbIL21, although this effect was less pronounced for K-IL15-K-IL21–expanded NK cells, suggesting some imprinting from the first exposure to mbIL15 (**Fig. 4A**). Glycolytic capacity, as defined by the ECAR responding to oligomycin treatment, trended higher in K-IL15–expanded NK cells (**Fig. 4B**). Plotting OCR versus ECAR for resting and stressed NK cells revealed that cells expanded with K-WT and K-IL15 were the most energetic, whereas the reduced metabolic activity in NK cells expanded by regimens containing mbIL21 was revealed by their "quiescent-like" metabolic state (**Fig. 4C**). Furthermore, only K-IL15–expanded NK cells possessed a superior ability to replenish ATP from glycolysis (**Fig. 4D**), suggesting a causal link between IL15 signaling and glycolytic energy production in the absence of IL21 signaling. Analysis of the mitochondrial membrane potential, a measure of metabolic robustness showed nonsignificant trends to an increase in NK cells expanded with K-IL15 or K-IL21-K-IL15 (**Fig. 4E**). Next, we examined measures of nutrient uptake. The glucose uptake assay showed modestly greater glucose uptake for K-IL15– over K-IL21–expanded NK cells, and for K-IL21-K-IL15 over K-IL15-K-IL21 expanded NK cells (**Fig. 4F**). Using the glycolysis inhibitor 2-DG, we found NK cells expanded with K-IL15 were less dependent on glycolysis for cytotoxicity than those expanded with K-IL21 (**Fig. 4G**). Finally, we found increased expression of nutrient transporters, including branched-chain and aromatic amino acid transporter (CD98) and transferrin (CD71), for K-IL15– and K-IL21-K-IL15–expanded NK cells (**Fig. 4H** and **I**), which might contribute to improved nutrient flexibility.

Feeder cell expansion conditions imprint distinct transcriptomic profiles of expanded NK cells

The transcriptomic profiles of the fresh and expanded NK cells from four donors were investigated via principal component analysis (PCA)

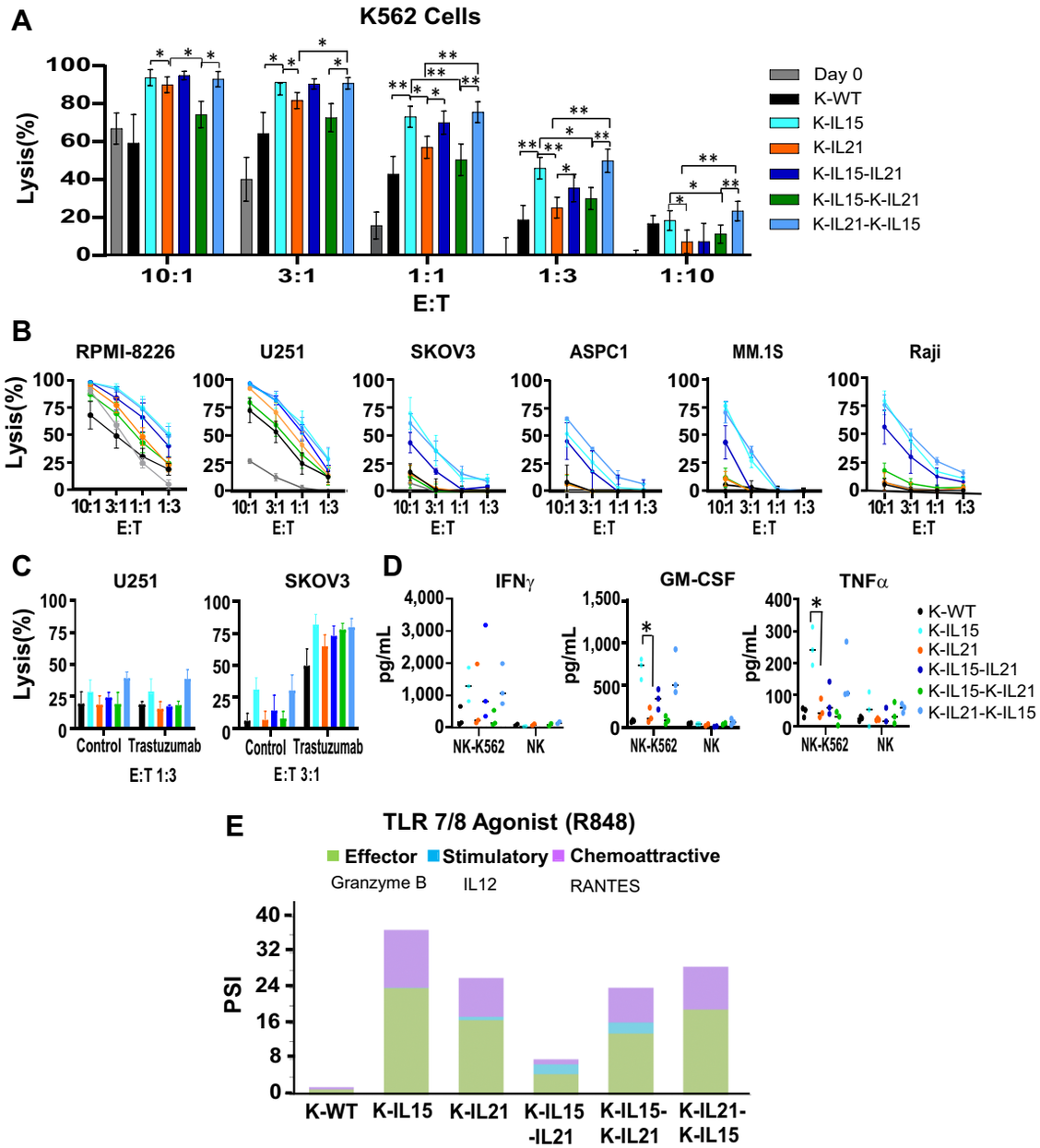

Figure 3.

Constant K-IL15 exposure or sequential K-IL21 and then K-IL15 drives greater NK cytotoxicity. Cytotoxicity of NK cells against K562 cells (9–10 donors; **A**), U251 cells (7 donors), RPMI-8226 cells (5 donors), SKOV3 cells (3 donors), ASPC1(3 donors), MM.1S cells (3 donors), and Raji cells (3 donors; **B**) was assessed by luciferase activity during coculture with tumor cells at different E:T ratio for 24 hours. The results are expressed as mean ± SE; *, $P < 0.05$ and **, $P < 0.01$ by fitting mixed model with multiple paired *t* test. **C,** ADCC of NK cells was assessed by luciferase activity during coculture with U251 or SKOV3 cells in the presence of or absence of trastuzumab 2 μg/mL for 24 hours (5 donors). **D,** The secretion of cytokine GMCSF and TNFa by expanded NK cells during coculture with K562 cells for 24 hours (3 donors). *, $P < 0.05$ by two-way ANOVA with multiple paired *t* test. **E,** PSI of expanded NK cells. The Isoplexis single-cell 32-plex Secretome Assay was performed to expanded NK cells after restimulation with TLR7/8 agonist (R848) 1 μg/mL overnight.

of bulk RNA-seq profiles. NK cells expanded with genetically engineered K562 feeder cells clustered separately from freshly isolated NK cells and those expanded with K-WT, despite large donor-to-donor variation in the latter (**Fig. 5A**, top). Comparing K-IL15– and K-IL21–expanded NK cells, we observed two distinct clusters with less donor-to-donor variation among K-IL15–expanded NK cells (**Fig. 5A**, bottom). Next, we compared the transcriptional profiles of expanded NK cells via Pearson correlation analysis. Freshly isolated NKs and those expanded with K-WT showed the greatest differences, both to each other and to NKs expanded with any of the genetically engineered K562 cells (Supplementary Fig. S7A and S7B). Among the NK cells expanded with engineered K562 feeder cells, there was less differential, but K-IL15

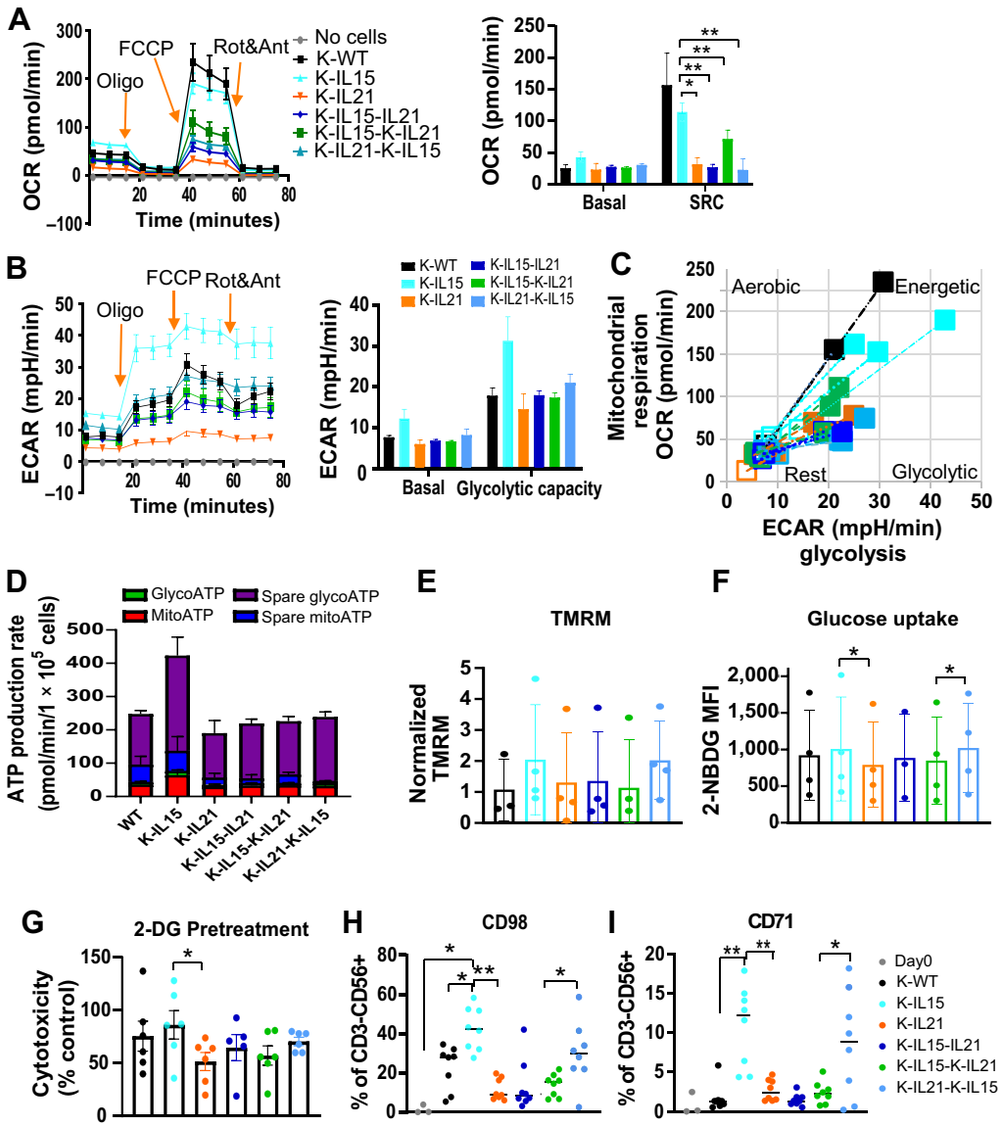

Figure 4.

Metabolic profiles of NK cells expanded under different conditions. Representative (left) and summarized (right) OCR (**A**) and ECAR (**B**) of expanded NK cells simultaneously measured in Seahorse Cell Stress Test. Basal OCR is the measurement before adding Oligo, and SRC is the difference of OCR between maximal measurement (after adding FCCP) and the basal measurement. Basal ECAR is the measurement before adding oligo and glycolytic capacity was the measurement of ECAR after adding Oligo. **C,** OCR versus ECAR under resting and stress conditions. **D,** ATP production rate by mitochondrial respiration and glycolysis. All the summarized data of Seahorse assays are from 3 donors. **E,** The mitochondrial membrane potential of NK cells was detected by MitoProbe TMRM Assay ($N = 4$ donors). **F,** Glucose uptake of NK cells was measured by 2-NBDG fluorescent tracer ($N = 4$ donors). **G,** The normalized cytotoxicity of NK cells pretreated with glycolysis inhibitor, 2-DG. The cytotoxicity of expanded NK cells against K562 was assessed by luciferase assay after pretreating NK cells with 2-DG 20 mmol/L overnight ($N = 5$ donors). The surface expression of CD98 (**H**) and CD71 (**I**) on NK cells was detected by flow cytometry ($N = 8$). The results are expressed as mean ± SE. *, $P < 0.05$ and **, $P < 0.01$ by two-way ANOVA with multiple paired t tests or one-way ANOVA with paired t tests.

and K-IL21 were the most distinct groups (Supplementary Fig. S7A and S7B). Matching our other phenotypic and functional data, NK cells expanded with K-IL21-K-IL15 showed the most similarity with NK cells expanded with K-IL15, whereas NK cells expanded with either K-IL15-K-IL21 or K-IL15-IL21 showed the most similarity with NK cells expanded with K-IL21 (Supplementary Fig. S7A and S7B), again highlighting a dominant effect of mbIL21. Focusing on K-IL15 versus K-IL21, in the two most differential groups among those stimulated with engineered K562 cells, we identified a total of 385 differentially expressed genes ($P_{adj} > 0.05$; $\log_2$ fold-change>2) when donors were pooled, with 234 upregulated and 151 downregulated transcripts (**Fig. 5B**). GSEA with Kyoto Encyclopedia of Genes and Genomes revealed 75 gene sets were enriched (normalized enrichment score ≥ 1.5; PDR <25%) and 3 gene sets were downregulated in K-IL15–expanded NK cells compared with K-IL21–expanded NK cells (Supplementary Fig. S7C). In line with the activation phenotype and greater cytotoxicity

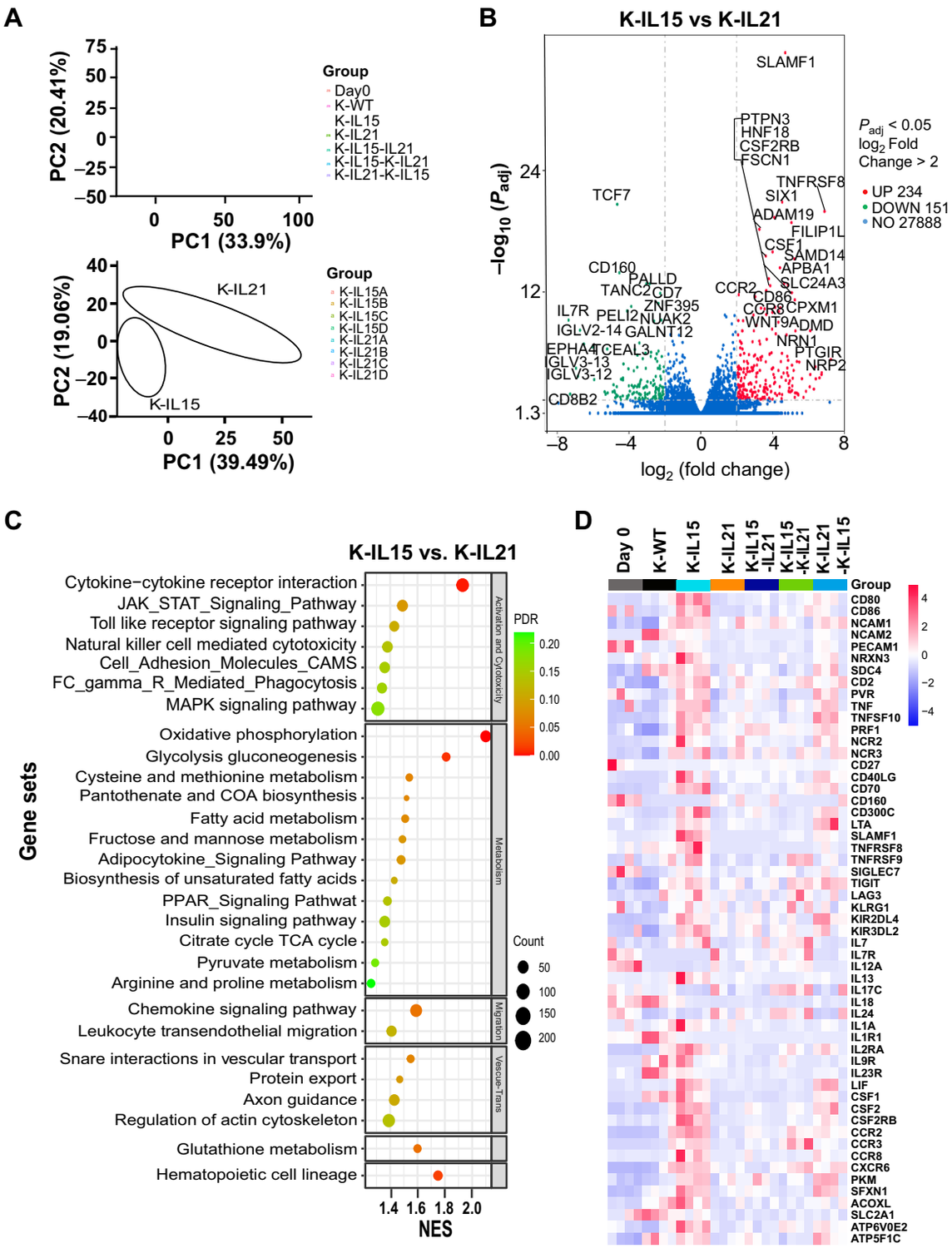

Figure 5.

Transcriptional profiles of NK cells expanded under different conditions. **A,** PCA of the expression profiles from the bulk RNA-seq of 4 donors' samples for seven groups (top) and K-IL15 and K-IL21 groups (bottom). **B,** Volcano plot for the differentially expressed genes ($P_{adj} > 0.05$; $\log_2$ fold change >2) in samples from all four donors in the K-IL15 versus K-IL21 group. **C,** Bubble plot of the selected gene sets enriched in K-IL15–expanded NK cells versus K-IL21–expanded NK cells. NES, normalized enrichment score. **D,** Heat map of normalized expression of both upregulated and downregulated genes differentially expressed from bulk RNA-seq. Each column represents one donor.

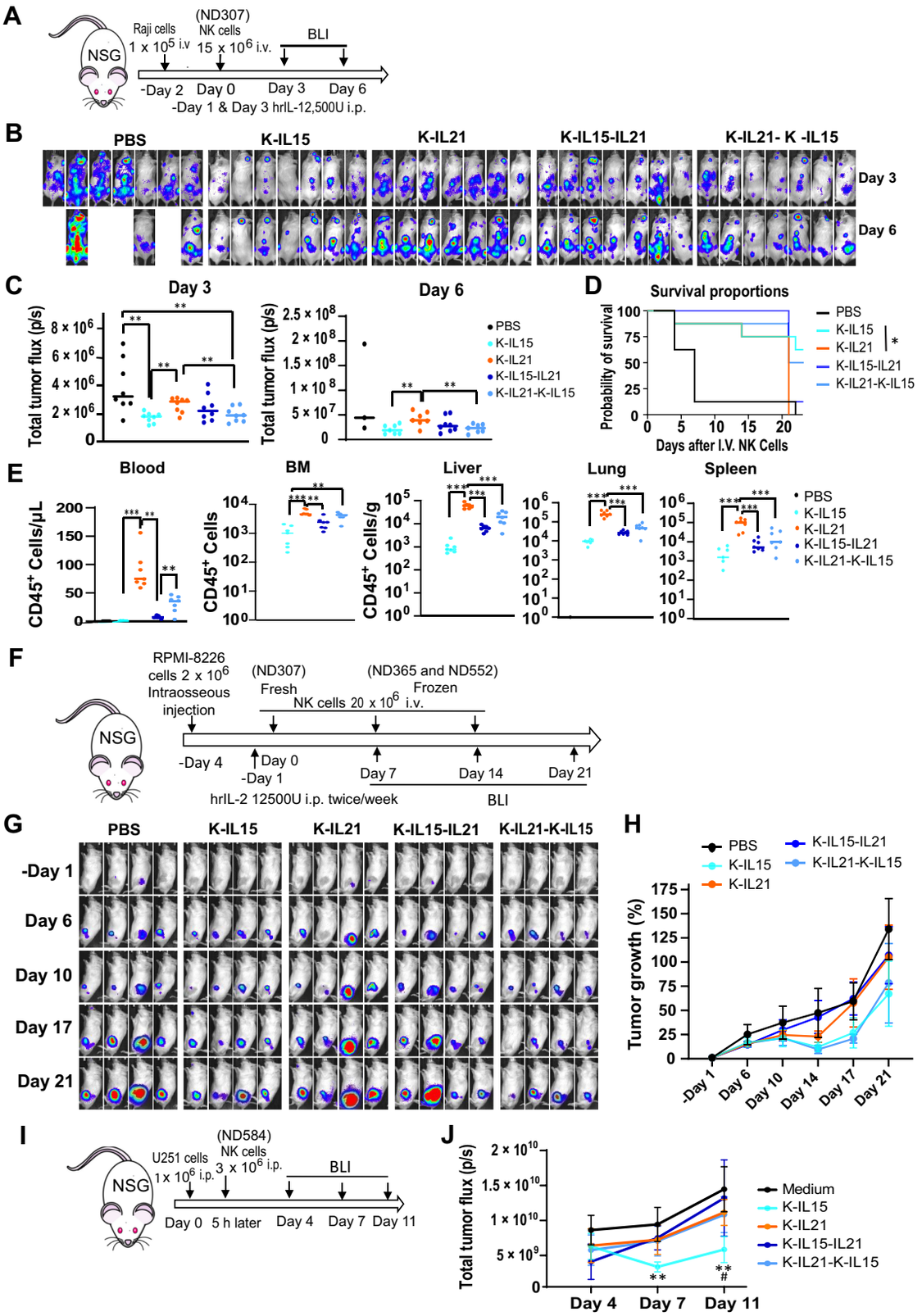
A
NSG
Raji cells
1 x 10^5 i.v
(ND307)
NK cells
15 x 10^6 i.v.
BLI
-Day 2
Day 0
Day 3
Day 6
-Day 1 & Day 3 hrIL-12,500U i.p.
B
PBS
K-IL15
K-IL21
K-IL15-IL21
K-IL21- K -IL15
Day 3
Day 6
C
Day 3
Day 6
Total tumor flux (p/s)
PBS
K-IL15
K-IL21
K-IL15-IL21
K-IL21-K-IL15
D
Survival proportions
Probability of survival
Days after I.V. NK Cells
PBS
K-IL15
K-IL21
K-IL15-IL21
K-IL21-K-IL15
E
Blood
BM
Liver
Lung
Spleen
CD45+ Cells/μL
CD45+ Cells
CD45+ Cells/g
F
RPMI-8226
cells 2 x 10^6
Intraosseous
injection
(ND307)
Fresh
(ND365 and ND552)
Frozen
NK cells 20 x 10^6 i.v.
NSG
-Day 4
Day 0
-Day 1
Day 7
Day 14
Day 21
hrIL-2 12500U i.p. twice/week
BLI
G
PBS
K-IL15
K-IL21
K-IL15-IL21
K-IL21-K-IL15
-Day 1
Day 6
Day 10
Day 17
Day 21
H
PBS
K-IL15
K-IL21
K-IL15-IL21
K-IL21-K-IL15
Tumor growth (%)
-Day 1
Day 6
Day 10
Day 14
Day 17
Day 21
I
NSG
U251 cells
1 x 10^6 i.p.
(ND584)
NK cells
3 x 10^6 i.p.
BLI
Day 0
5 h later
Day 4
Day 7
Day 11
J
Total tumor flux (p/s)
Medium
K-IL15
K-IL21
K-IL15-IL21
K-IL21-K-IL15
Day 4
Day 7
Day 11

of NK cells expanded with K-IL15, NK activation and cytotoxicity-related gene sets (cytokine–cytokine receptor interaction, cell adhesion molecules, TLR-JAK-STAT- and NOD-like receptor signaling pathways, NK cell–mediated cytotoxicity, and Fc gamma receptor-mediated phagocytosis) were enriched in K-IL15–expanded NK cells compared with K-IL-21–expanded NK cells (**Fig. 5C** and **D**). Chemokine signaling and leukocyte transendothelial migration were also enriched in K-IL15–expanded NK cells compared with K-IL21–expanded NK cells (**Fig. 5C** and **D**), suggesting they might be better able to migrate to and act within tumor lesions. Consistent with the metabolic profile, K-IL15–expanded NK cells showed enrichment in the multiple metabolism-related gene sets, including oxidative phosphorylation, insulin signaling, glycolysis/gluconeogenesis, fatty acid metabolism, and arginine and proline metabolism (**Fig. 5C**). Pyruvate kinase isozymes (PKM; involved in the last step of glycolysis), SFXN1 (a mitochondrial serine transporter required for one-carbon metabolism), and acyl-CoA oxidase like (ACOXL; involved in fatty acid beta-oxidation) were highly upregulated in K-IL15–expanded NK cells (**Fig. 5D**). In addition, the gene sets for hematopoietic cell lineage, regulation of actin cytoskeleton, axon guidance, SNARE interaction in vesicular transport, and glutathione metabolism were enriched in K-IL15–expanded NK cells compared with K-IL21–expanded NK cells (**Fig. 5C**). Sequential exposure to K-IL21-K-IL15 showed a similar gene expression profile to constant exposure to K-IL15 (**Fig. 5D**), in line with our phenotypic and functional data.

Feeder cell expansion conditions affect the *in vivo* function of expanded NK cells

To investigate the *in vivo* antitumor efficacy of the expanded NK cells, we used three xenograft models in NSG mice, utilizing three separate tumor entities with varying sensitivity to fresh NK cells (**Fig. 3B**): Raji (Burkitt lymphoma), RPMI-8226 (multiple myeloma), and U251 (glioblastoma) cells. Tumor cells were administered into three different compartments: the blood, bone marrow, and peritoneum, respectively, to test the ability of NK cells expanded under different conditions to meet a variety of challenges, including (i) disseminated (Raji intravenous model) or localized (RPMI-8226 intraosseous and U251 intraperitoneal models) disease, (ii) varying need for NK cell migration from high (RPMI-8226 intraosseous model) to low (U251 intraperitoneal model), and (iii) varying cytokine support from modest (12,500 IU IL2 twice weekly in Raji and RPMI-8226 models) to none (U251 intraperitoneal carcinomatosis model). NK cells expanded with K-WT or K-IL15-K-IL21 were not studied *in vivo* due to low yield and poor *in vitro* functionality. In the Raji disseminated disease model, the tumor burden rapidly advanced in the PBS-treated group, with mice starting to reach humane endpoints in a little over a week after Raji cell injection (**Fig. 6A** and **B**). NK cells expanded with K-IL15 or K-IL21-K-IL15 showed significantly better tumor control compared with NK cells expanded with K-IL21 (**Fig. 6B** and **C**). On day 21, all mice in K-IL21 and 7 of 8 mice in K-IL15-IL21 group reached humane endpoints, whereas over 50% of mice in the K-IL15 and K-IL21-K-IL15 groups survived (**Fig. 6D**). NK cells expanded with K-IL21 also showed better expansion *in vivo* but despite this, showed inferior tumor control (**Fig. 6E**), consistent with being programmed for proliferation but relatively metabolically quiescent (**Figs. 1** and **4**). In the RPMI-8226 intraosseous multiple myeloma model on day 14 after NK cell infusion, mice receiving NK cells from K-IL15, K-IL21, and K-IL21-KIL15 expansions started to exhibit a trending reduction in the rate of tumor growth, whereas mice in K-IL15-IL21 group did not (**Fig. 6F–H**). On day 17 day after the first NK cell infusion, mice treated with NK cells from K-IL15 and K-IL21-KIL15 conditions sustained trends toward tumor control, whereas NK cells from K-IL21 did not (**Fig. 6G** and **H**). By day 21, 7 days after the last of three NK injections, tumors were growing in all mice, although groups treated with NK cells expanded by K-IL15 and K-IL21-K-IL15 had grown the least (**Fig. 6F–H**). Next, we tested the expanded NK cells in the U251 cell carcinomatosis model without cytokine support and found only mice treated with K-IL15–expanded NK cells showed temporary tumor control (**Fig. 6I** and **J**). Together our *in vivo* models showed equal and significant control by K-IL15– and K-IL21-K-IL15–expanded NK cells in the aggressive disseminated Raji model; an equal trend to control in the intraosseous RPMI-8226 model; and control by only K-IL15–expanded NK cells in the U251 peritoneal carcinomatosis model. We could find only trends for *in vivo* activity for NK cells expanded with K-IL21 or K-IL15-IL21 in any of these models.

Discussion

Expansion of NK cells from the healthy adult donor or umbilical cord blood using feeder cells engineered to express mbIL15 and/or mbIL21 is a common approach for obtaining sufficient NK cells for clinical trials (6–12), but the differential and especially the sequential use of these mb cytokines has not been adequately explored. In keeping with prior reports (7, 11), we found that feeder cells expressing mbIL21 drove significantly greater NK cell yields and differential transcriptomes compared with those expressing mbIL15, whereas exposure to either or both cytokines increased NK cytotoxicity compared to freshly isolated–expanded or K-WT–expanded NK cells. However, we found that exposure to mbIL15 alone or for the second of two feeder cell stimulations led to greater breadth and potency of natural cytotoxicity, superior polyfunctional cytokine production, and *in vivo* tumor control. Furthermore, exposure to mbIL15 alone during NK expansion improved the metabolic fitness of the resulting NK cells, including their ability to acquire and use nutrients. Some improvements in nutrient acquisition capacity were also observed for the sequence mbIL21 followed by mbIL15; however, exposure to mbIL21 in most

Figure 6.

In vivo antitumor efficacy of NK cells expanded from different conditions in various mouse tumor models. Schematic diagram of the timeline (**A**), tumor bioluminescence images (**B**), quantification (**C**), mouse survival curves (**D**), and blood and tissue NK cells (**E**) of the mouse Burkitt lymphoma model. NSG mice were intravenously (i.v.) injected with Raji-CBG cells (1e5/mouse) followed by intravenous injection with frozen expanded NK cells (15e6 cells/mouse) 2 days later (8 mice/group). Blood and tissue NK cells were measured on day 4 after NK cell injection in another experiment. **, $P < 0.01$; and ***, $P < 0.001$ by one-way ANOVA with *t* test. *, $P < 0.05$ by survival analysis (Kaplan–Meier). Schematic diagram of the timeline (**F**), tumor bioluminescence images (**G**), and the summarized tumor growth (**H**) of the mouse multiple myeloma model. NSG mice received an intraosseous injection of RPMI8226-CBG (2e6 cells/mouse) following busulfan preconditioning. Expanded NK cells (20e6/mouse) from 3 donors were delivered by intravenous injection weekly for 3 weeks (6 mice/group). Human rIL2 (12,500 IU/mouse) was intraperitoneally delivered to the mice twice per week for both the lymphoma and multiple myeloma models. Schematic diagram of the timeline (**I**) and tumor flux (**J**) of the peritoneal carcinomatosis mouse model. NSG mice received intraperitoneal injection with U251-CBG cells (1e6 cells/mouse) and then freshly expanded NK cells (3e6 cells/mouse) were given 5 hours later (10 mice/group, except for 5 mice in the K-IL15-IL21 due to low yield for that expansion). The results are expressed as mean ± SE. **, $P < 0.01$ versus Medium group; and # $P < 0.05$ versus K-IL21 group by two-way ANOVA with multiple *t* tests.

contexts resulted in NK cells with less robust metabolism. In our study, sequential stimulus with mbIL21 followed by mbIL15 generated far higher yields of NK cells than stimulus with mbIL15-based feeders alone, but with equivalent *in vivo* activity in the disseminated Raji model and the intraosseous RPMI-8226 model. It is tempting to speculate whether an extended period of mbIL15 stimulation might allow the metabolism of NK cells first exposed to mbIL21 to mirror those only exposed to mbIL15 in all respects, and this will be an area of further study. Our data further showed that the choice of mbIL15 and/or mbIL21 did not affect ADCC capacity.

We observed that across multiple assays, including the phenotype by 28-color flow cytometry, cytotoxic breadth and potency, cytokine secretome, metabolic profile, transcriptome, and activity in a xenograft model, NK cells expanded with mbIL21 followed by mbIL15 were most like those expanded with mbIL15 alone. Meanwhile, NK cells expanded with mbIL15 together with or followed by mbIL21 were generally more like those expanded with mbIL21 alone. These findings suggest that NK cells possess sufficient flexibility to reshape their phenotype and function in response to the most recent stimulus, be it mbIL15 or mbIL21, but that the effects of mbIL21 are generally dominant when used together. In this manner, an important novel finding of our study concerns the sequential use of mbIL21 feeder cells followed by those expressing mbIL15. This sequence enabled yields only marginally lower than those obtained with consistent mbIL21 stimulation, with the benefit that the resulting NK cells possessed nearly all the superior antitumoral functional properties imparted by exposure to mbIL15 alone.

On the basis of our findings, aside from where NK cells are used exclusively for ADCC where yield may be the only consideration, the use of mbIL21 followed by mbIL15 feeder cells might be the optimal choice due to the high yield and improved functionality. It is tempting to speculate about CAR-NK cells that coexpress mbIL15 and whether expanding these with mbIL21 feeder cells would be optimal. The landmark CD19 CAR-NK study of Liu and colleagues (35) used mbIL21 feeder cell–based expansion followed by transduction of the NK cells with mbIL15 alongside the CAR and then restimulation with the mbIL21 feeder cells (36). In this context, the sequence would be mbIL21 followed by mbIL15 and mbIL21 in combination, a sequence that we have not studied, although we would predict it might be suboptimal. However, it could be that with CAR-NK cells, the activation signal via the CAR is dominant, as it was for antibody in our ADCC assay. Even if this is the case, prevention of antigen-negative tumor escape both via the natural cytotoxicity of NK cells and via their ability to orchestrate broader antitumoral immune responses (3, 4) might still justify seeking the most functional NK cells in a CAR-NK cell process.

Authors' Disclosures

R.S. O'Connor reports grants from NIH during the conduct of the study; other support from Nucleus Biologics outside the submitted work. J.L. Riley reports grants from NIH during the conduct of the study; grants from Tmunity/Kite outside the submitted work; in addition, J.L. Riley has a patent for "Anti-CD3 scFv and cytokine producing artificial antigen presenting cells" pending to University of Pennsylvania. N.C. Sheppard reports personal fees from Outpace Bio and Immunai Inc outside the submitted work. No disclosures were reported by the other authors.

Authors' Contributions

C. Zhang: Conceptualization, data curation, formal analysis, supervision, investigation, methodology, writing–original draft, writing–review and editing. **S. Kadu:** Investigation. **Y. Xiao:** Investigation. **O. Johnson:** Investigation. **A. Kelly:** Investigation. **R.S. O'Connor:** Resources, formal analysis, supervision, funding acquisition, methodology, writing–original draft. **M. Lai:** Investigation. **H. Kong:** Investigation. **S. Srivatsa:** Investigation. **V. Tai:** Investigation. **E. Greenblatt:** Investigation. **M. Holmes:** Investigation, methodology. **J.L. Riley:** Resources, supervision. **C.H. June:** Resources, supervision. **N.C. Sheppard:** Conceptualization, supervision, methodology, writing–original draft, project administration, writing–review and editing.

Acknowledgments

This work was supported by UPenn private funds (C. Zhang, S. Kadu, Y. Xiao, O. Johnson, A. Kelly, C.H. June, M. Lai, H. Kong, S. Srivatsa, V. Tai, N.C. Sheppard), NIH R01 CA226983 (C.H. June, R.S. O'Connor), and Ludwig Research Foundation (Princeton Branch; R.S. O'Connor).

The authors wish to thank Krishna Vijayendran for assistance with analysis of 28-color flow cytometry and Linhui Chen for assistance with Bulk RNA-seq data analysis. The authors also thank Lynn Chen, Max Eldabbas, and Emileigh Maddox of the Human Immunology Core at the Perelman School of Medicine at the University of Pennsylvania for providing purified human NK cells. The HIC is supported in part by NIH P30 AI045008 and P30 CA016520. HIC RRID: SCR_022380.

The publication costs of this article were defrayed in part by the payment of publication fees. Therefore, and solely to indicate this fact, this article is hereby marked "advertisement" in accordance with 18 USC section 1734.

Note

Supplementary data for this article are available at Cancer Immunology Research Online (http://cancerimmunolres.aacrjournals.org/).

Received February 18, 2023; revised June 14, 2023; accepted August 28, 2023; published first August 30, 2023.

References

1. Laskowski TJ, Biederstadt A, Rezvani K. Natural killer cells in antitumour adoptive cell immunotherapy. Nat Rev Cancer 2022;22:557–75.
2. Yoon SR, Kim TD, Choi I. Understanding of molecular mechanisms in natural killer cell therapy. Exp Mol Med 2015;47:e141.
3. Böttcher JP, Bonavita E, Chakravarty P, Blees H, Cabeza-Cabrerizo M, Sammicheli S, et al. NK cells stimulate recruitment of cDC1 into the tumor microenvironment promoting cancer immune control. Cell 2018;172:1022–37.
4. Kirchhammer N, Trefny MP, Natoli M, Brücher D, Smith SN, Werner F, et al. NK cells with tissue-resident traits shape response to immunotherapy by inducing adaptive antitumor immunity. Sci Transl Med 2022;14:eabm9043.
5. Robertson MJ, Ritz J. Biology and clinical relevance of human natural killer cells. Blood 1990;76:2421–38.
6. Lapteva N, Durett AG, Sun J, Rollins LA, Huye LL, Fang J, et al. Large-scale *ex vivo* expansion and characterization of natural killer cells for clinical applications. Cytotherapy 2012;14:1131–43.
7. Denman CJ, Senyukov VV, Somanchi SS, Phatarpekar PV, Kopp LM, Johnson JL, et al. Membrane-bound IL-21 promotes sustained *ex vivo* proliferation of human natural killer cells. PLoS One 2012;7:e30264.
8. Fujisaki H, Kakuda H, Shimasaki N, Imai C, Ma J, Lockey T, et al. Expansion of highly cytotoxic human natural killer cells for cancer cell therapy. Cancer Res 2009;69:4010–7.
9. Imai C, Iwamoto S, Campana D. Genetic modification of primary natural killer cells overcomes inhibitory signals and induces specific killing of leukemic cells. Blood 2005;106:376–83.
10. Gurney M, Kundu S, Pandey S, O'Dwyer M. Feeder cells at the interface of natural killer cell activation, expansion and gene editing. Front Immunol 2022;13:802906.
11. Chang M, Tang X, Nelson L, Nyberg G, Du Z. Differential effects on natural killer cell production by membrane-bound cytokine stimulations. Biotechnol Bioeng 2022;119:1820–38.

12. Liu E, Ang SOT, Kerbauy L, Basar R, Kaur I, Kaplan M, et al. GMP-compliant universal antigen presenting cells (uAPC) promote the metabolic fitness and antitumor activity of armored cord blood CAR-NK cells. Front Immunol 2021; 12:626098.
13. Gotthardt D, Trifinopoulos J, Sexl V, Putz EM. JAK/STAT cytokine signaling at the crossroad of NK cell development and maturation. Front Immunol 2019;10: 2590.
14. Barrett DM, Liu X, Jiang S, June CH, Grupp SA, Zhao Y. Regimen-specific effects of RNA-modified chimeric antigen receptor T cells in mice with advanced leukemia. Hum Gene Ther 2013;24:717–27.
15. Good CR, Aznar MA, Kuramitsu S, Samareh P, Agarwal S, Donahue G, et al. An NK-like CAR T cell transition in CAR T cell dysfunction. Cell 2021;184:6081–100.
16. Liu X, Jiang S, Fang C, Yang S, Olalere D, Pequignot EC, et al. Affinity-tuned ErbB2 or EGFR chimeric antigen receptor T cells exhibit an increased therapeutic index against tumors in mice. Cancer Res 2015;75:3596–607.
17. Chu Y, Yahr A, Huang B, Ayello J, Barth M, S. Cairo M. Romidepsin alone or in combination with anti-CD20 chimeric antigen receptor expanded natural killer cells targeting Burkitt lymphoma in vitro and in immunodeficient mice. Oncoimmunology 2017;6:e1341031.
18. Poznanski SM, Singh K, Ritchie TM, Aguiar JA, Fan IY, Portillo AL, et al. Metabolic flexibility determines human NK cell functional fate in the tumor microenvironment. Cell Metab 2021;33:1205–20.
19. Brummelman J, Haftmann C, Núñez NG, Alvisi G, Mazza EMC, Becher B, et al. Development, application and computational analysis of high-dimensional fluorescent antibody panels for single-cell flow cytometry. Nat Protoc 2019; 14:1946–69.
20. Singh H, Figliola MJ, Dawson MJ, Huls H, Olivares S, Switzer K, et al. Reprogramming CD19-specific T cells with IL-21 signaling can improve adoptive immunotherapy of B-lineage malignancies. Cancer Res 2011;71:3516–27.
21. Suhoski MM, Golovina TN, Aqui NA, Tai VC, Varela-Rohena A, Milone MC, et al. Engineering artificial antigen-presenting cells to express a diverse array of co-stimulatory molecules. Mol Ther 2007;15:981–8.
22. Sun M, Fink PJ. A new class of reverse signaling costimulators belongs to the TNF family. J Immunol 2007;179:4307–12.
23. Carbone E, Ruggiero G, Terrazzano G, Palomba C, Manzo C, Fontana S, et al. A new mechanism of NK cell cytotoxicity activation: the CD40-CD40 ligand interaction. J Exp Med 1997;185:2053–60.
24. Jung D, Baek YS, Lee IJ, Kim KY, Jang H, Hwang S, et al. *Ex vivo* expanded allogeneic natural killer cells have potent cytolytic activity against cancer cells through different receptor-ligand interactions. J Exp Clin Cancer Res 2021;40: 333.
25. Poli A, Michel T, Thérésine M, Andrès E, Hentges F, Zimmer J. CD56bright natural killer (NK) cells: an important NK cell subset. Immunology 2009;126: 458–65.
26. Lieberman NAP, DeGolier K, Haberthur K, Chinn H, Moyes KW, Bouchlaka MN, et al. An uncoupling of canonical phenotypic markers and functional potency of *ex vivo*-expanded natural killer cells. Front Immunol 2018;9:150.
27. Poznanski SM, Nham T, Chew MV, Lee AJ, Hammill JA, Fan IY, et al. Expanded CD56(superbright)CD16(+) NK cells from ovarian cancer patients are cytotoxic against autologous tumor in a patient-derived xenograft murine model. Cancer Immunol Res 2018;6:1174–85.
28. Wagner JA, Rosario M, Romee R, Berrien-Elliott MM, Schneider SE, Leong JW, et al. CD56bright NK cells exhibit potent antitumor responses following IL-15 priming. J Clin Invest 2017;127:4042–58.
29. Peruzzi G, Femnou L, Gil-Krzewska A, Borrego F, Weck J, Krzewski K, et al. Membrane-type 6 matrix metalloproteinase regulates the activation-induced downmodulation of CD16 in human primary NK cells. J Immunol 2013;191: 1883–94.
30. Romee R, Foley B, Lenvik T, Wang Y, Zhang B, Ankarlo D, et al. NK cell CD16 surface expression and function is regulated by a disintegrin and metalloprotease-17 (ADAM17). Blood 2013;121:3599–608.
31. Haining WN. Travels in time: assessing the functional complexity of T cells. Proc Natl Acad Sci U S A 2012;109:1359–60.
32. Rossi J, Paczkowski P, Shen Y-W, Morse K, Flynn B, Kaiser A, et al. Preinfusion polyfunctional anti-CD19 chimeric antigen receptor T cells are associated with clinical outcomes in NHL. Blood 2018;132:804–14.
33. Terrén I, Orrantia A, Vitallé J, Astarloa-Pando G, Zenarruzabeitia O, Borrego F. Modulating NK cell metabolism for cancer immunotherapy. Semin Hematol 2020;57:213–24.
34. van der Windt GJW, Chang CH, Pearce EL. Measuring bioenergetics in T cells using a seahorse extracellular flux analyzer. Curr Protoc Immunol 2016;113: 3.16B.1–3.16B.14.
35. Liu E, Marin D, Banerjee P, Macapinlac HA, Thompson P, Basar R, et al. Use of CAR-transduced natural killer cells in CD19-positive lymphoid tumors. N Engl J Med 2020;382:545–53.
36. Liu E, Tong Y, Dotti G, Shaim H, Savoldo B, Mukherjee M, et al. Cord blood NK cells engineered to express IL-15 and a CD19-targeted CAR show long-term persistence and potent antitumor activity. Leukemia 2018;32:520–31.